Low-energy collective excitations in the neutron star inner crust

N. Chamel,[1] D. Page,[2] and S. Reddy[3]
[1]*Institut d'Astronomie et d'Astrophysique, Université Libre de Bruxelles CP226, 1050 Brussels, Belgium*
[2]*Instituto de Astronomía, Universidad Nacional Autonóma de México, Mexico D.F. 04510, Mexico*
[3]*Institute for Nuclear Theory, University of Washington, Seattle, Washington 98195, USA*
(Received 16 October 2012; revised manuscript received 13 February 2013; published 25 March 2013)

We study the low-energy collective excitations in the inner crust of the neutron star, where a neutron superfluid coexists with a Coulomb lattice of nuclei. The dispersion relation of the modes is calculated systematically from a microscopic theory including neutron band structure effects. These effects are shown to lead to a strong mixing between the Bogoliubov-Anderson bosons of the neutron superfluid and the longitudinal crystal lattice phonons. In addition, the speed of the transverse shear mode is greatly reduced as a large fraction of superfluid neutrons are entrained by nuclei. Not only does the much smaller velocity of the transverse mode increase the specific heat of the inner crust, it also decreases its electron thermal conductivity. These results may impact our interpretation of the thermal relaxation in accreting neutron stars. Due to strong mixing, the mean free path of the superfluid mode is found to be greatly reduced. Our results for the collective mode dispersion relations and their damping may also have implications for neutron star seismology.

DOI: 10.1103/PhysRevC.87.035803 PACS number(s): 26.60.Gj, 21.65.−f, 47.37.+q, 97.60.Jd

I. INTRODUCTION

The crust of a neutron star represents only about 10% of the star's radius and 1% of its mass but is expected to play a key role in various observed astrophysical phenomena such as pulsar glitches, quasiperiodic oscillations in soft gamma repeaters (SGRs), and thermal relaxation in soft x-ray transients [1]. The outer crust is primarily composed of pressure-ionized atoms arranged in a regular crystal lattice and embedded in a highly degenerate electron gas. With increasing density, electrons become relativistic and the rapid growth of their Fermi energy drives nuclei to become neutron rich due to electron captures (see, e.g., Ref. [2]). Eventually, at a density $\sim 4 \times 10^{11}$ g/cm^3, some neutrons drip out of nuclei (see, e.g., Refs. [3,4]). This defines the boundary between the outer crust and the inner crust. "Dripped" neutrons in the inner crust are expected to become superfluid below a critical temperature of the order of $\sim 10^{10}$ K (see, e.g., Ref. [5]). Despite the absence of viscous drag, the neutron superfluid can still be coupled to the crust due to nondissipative entrainment effects arising from elastic Bragg scattering of dripped neutrons by the crystal lattice [6,7]. Recent calculations have shown that in some regions of the inner crust only a very small fraction of dripped neutrons participate in the superfluid dynamics [8,9]. Consequently, the vibrations of the crystal lattice are expected to be strongly coupled to the collective excitations of the neutron superfluid [10–12]. Collective excitations are particularly important for understanding thermal and transport properties of accreting neutron stars with temperatures in the range $T = 10^7$–10^9 K [13].

In this paper, we study low-energy collective modes with large wavelengths compared to the typical internuclei distance. The existence of two longitudinal modes in the inner crust and the role of entrainment in determining the dispersion relations were first studied in Ref. [14] using a hydrodynamic approach. In this pioneering study, long-range perturbations on the superfluid flow induced by the lattice of nuclei were neglected. Here we show that they play a crucial role. The low-energy constants that depend on the microscopic properties of the inner crust are calculated in a consistent approach that properly incorporates the long-range correlations leading to entrainment effects, first discussed in Ref. [8]. We find that entrainment of superfluid neutrons by crustal nuclei greatly reduces the velocity of the two transverse (shear) modes, and this in turn enhances their contribution to the low-temperature specific heat of the inner crust. Entrainment effects also induce a strong mixing between the longitudinal lattice phonons and the Bogoliubov-Anderson (BA) bosons [15,16] of the neutron superfluid, splitting these modes into a high velocity global sound mode and a low velocity mode characterized by a relative motion between the neutron superfluid and the electron-ion plasma. These results should be also relevant for studies of global neutron star seismic modes with frequencies in the range 20–1000 Hz, which could be excited during violent events such as giant flares in SGRs and binary neutron-star mergers.

In the following section we define our notations and present order-of-magnitude estimates of the relevant length and momentum scales. In Sec. III we describe the low-energy, long-wavelength, collective excitation modes and their velocities. The microscopic model of Ref. [9] is employed in Sec. IV to obtain quantitive values for these velocities. Damping of these modes is briefly considered in Sec. V. In the Sec. VI we study how entrainment affects the inner crust specific heat, its thermal conductivity, and its thermal relaxation time scale. We finally conclude in Sec. VII.

II. BASIC NOTATIONS AND PHYSICAL SCALES

In what follows, we will assume that the inner crust of a neutron star is a perfect crystal. Each crustal layer will consist of a body-centered cubic lattice containing only one type of nuclide and will be characterized by Z, the *total* average number of protons in the Wigner-Seitz (W-S) cell of the crystal lattice (a truncated octahedron); $A_{\rm cell}$, the *total* cell

average number of nucleons; A, the cell average number of nucleons *bound* inside nuclei; and $A^\star$, the cell average number of nucleons *entrained* by the solid crust. As shown in Ref. [9], $A^\star$ is generally much larger than A and close to $A_{\rm cell}$ due to the Bragg scattering of unbound neutrons by the periodic potential of the crystal lattice, which manifests itself in neutron band structure effects.

We will indicate by $n = n_p + n_n$ the total average baryon number density, which is the sum of the average proton density n_p and average neutron density n_n. Neutrons entrained by nuclei are effectively bound. Their density will be noted as $n_n^{\rm b}$. By analogy with conduction electrons in ordinary solids, neutrons that are not entrained will be referred to as *conduction* neutrons and their density will be noted as $n_n^{\rm c}$. As shown in Ref. [9], the density $n_n^{\rm c}$ is generally much smaller than the density $n_n^{\rm f}$ of "free" or "dripped" neutrons. Because of Galilean invariance, we have

$$n_n = n_n^{\rm b} + n_n^{\rm c}. \tag{1}$$

These densities are related to Z, $A^\star$, and $A_{\rm cell}$ by

$$n_n^{\rm b} = \frac{A^\star - Z}{A_{\rm cell}}\, n \tag{2}$$

and

$$n_p = \frac{Z}{A_{\rm cell}}\, n. \tag{3}$$

The ion number density $n_{\rm I}$ is determined by

$$n_{\rm I} = \frac{n}{A_{\rm cell}}. \tag{4}$$

As discussed in Refs. [10–12], the mass density associated with lattice vibrations is given by

$$\rho_{\rm I} = m\left(n_p + n_n^{\rm b}\right) = A^\star m\, n_{\rm I}, \tag{5}$$

where m is the nucleon mass (neglecting the small difference between neutron and proton masses), whereas the total mass density (neglecting the electron contribution) is

$$\rho = m\, n = A_{\rm cell}\, m\, n_{\rm I}. \tag{6}$$

The typical length scale associated with the solid crust is the ion-sphere radius defined by

$$r_{\rm I} = \left(\frac{3}{4\pi n_{\rm I}}\right)^{1/3} \approx 75 \left(\frac{A_{\rm cell}/1000}{\rho_{12}}\right)^{1/3} \text{fm}, \tag{7}$$

where $\rho_{12} = \rho/(10^{12}\ \text{g cm}^{-3})$. The characteristic angular frequency and wave number of lattice vibrations is the ion angular plasma frequency

$$\omega_p = \sqrt{\frac{4\pi (Ze)^2 n_{\rm I}}{A^\star m}} = \sqrt{\frac{4\pi e^2 n_p^2}{\left(n_p + n_n^{\rm b}\right) m}} \tag{8}$$

and the Debye wave number

$$q_D = (6\pi^2 n_{\rm I})^{1/3} \approx \frac{2.4}{r_{\rm I}} \approx 0.03 \left(\frac{\rho_{12}}{A_{\rm cell}/1000}\right)^{1/3} \text{fm}^{-1}, \tag{9}$$

respectively. The ion plasma temperature is defined by $T_p = \hbar\omega_p/k_{\rm B}$ ($k_{\rm B}$ being the Boltzmann constant).

The ultrarelativistic electrons found in the inner crust of neutron stars with density $n_e = Z n_{\rm I}$, are almost uniformly distributed [17] and are characterized by their Fermi wave number

$$k_{\rm Fe} = (3\pi^2 n_e)^{1/3} = \left(\frac{Z}{2}\right)^{1/3} q_D \approx \frac{7}{r_{\rm I}} \left(\frac{Z}{50}\right)^{1/3} \approx 0.1 \left(\frac{\rho_{12}\ Z/50}{A_{\rm cell}/1000}\right)^{1/3} \text{fm}^{-1}. \tag{10}$$

Small deviations of the electron distribution from uniformity are characterized by the electron Thomas-Fermi screening wave number

$$q_{\rm TFe} = \sqrt{4\pi e^2 \frac{\partial n_e}{\partial \mu_e}} = \sqrt{\frac{4\alpha}{\pi}}\, k_{\rm Fe} \approx 0.1\, k_{\rm Fe} \approx \frac{0.7}{r_{\rm I}} \left(\frac{Z}{50}\right)^{1/3}, \tag{11}$$

where $\mu_e = \hbar c\, k_{\rm Fe}$ is the electron chemical potential and $\alpha \equiv e^2/\hbar c \approx 1/137$ the fine structure constant.

III. LOW-ENERGY DYNAMICS OF THE NEUTRON-STAR INNER CRUST

The equations governing the low-energy dynamics of a nonrelativistic neutron superfluid immersed in an elastic crust have been derived in Refs. [11,12,18]. The corresponding normal modes of oscillation can be found by considering small perturbations of the densities and currents from their equilibrium values and solving the resulting linearized hydrodynamic equations. The first two of these equations arise from the conservation of neutron and proton numbers

$$\frac{\partial \delta n_n}{\partial t} + n_n^{\rm c} \boldsymbol{\nabla} \cdot \delta \boldsymbol{v_n} + n_n^{\rm b} \boldsymbol{\nabla} \cdot \delta \boldsymbol{v_p} = 0, \tag{12}$$

$$\frac{\partial \delta n_p}{\partial t} + n_p \boldsymbol{\nabla} \cdot \delta \boldsymbol{v_p} = 0, \tag{13}$$

where δn_n and δn_p are the perturbed neutron and proton densities, respectively, while $\delta \boldsymbol{v_n}$ and $\delta \boldsymbol{v_p}$ are the perturbed neutron and proton velocities, respectively. In the following, we will consider oscillations characterized by wave vectors $q \ll q_{\rm TFe}$ so the crustal matter remains electrically neutral locally and $n_p = n_e$. Treating the neutron-star crust as an isotropic solid and using i, j, k for coordinate space indices, the momentum conservation can be expressed as

$$m n_n^{\rm c} \frac{\partial \delta v_{ni}}{\partial t} + \rho_{\rm I} \frac{\partial \delta v_{pi}}{\partial t} + n_n \nabla_i \delta\mu_n + L \nabla_i \delta n_n - \tilde{K} \nabla_i u_{jj} - 2S \nabla_j \left(u_{ij} - \delta_{ij} \frac{1}{3} u_{kk}\right) = 0, \tag{14}$$

where u_{ij} is the strain tensor, $\delta\mu_n$ the perturbed neutron chemical potential, S the shear modulus, and $\tilde{K}$ the bulk modulus of the electron-ion system

$$\tilde{K} = n_p^2 \left(\frac{\partial \mu_p}{\partial n_p} + \frac{\partial \mu_e}{\partial n_e}\right), \tag{15}$$

and the coefficient L given by

$$L = n_p \frac{\partial \mu_n}{\partial n_p} \tag{16}$$

takes into account the coupling of the neutron superfluid to the strain field. The condition for neutron superfluidity is embedded in Josephson's equation,

$$\frac{\partial \delta \boldsymbol{v_n}}{\partial t} + \frac{1}{m} \boldsymbol{\nabla} \delta \mu_n = 0. \tag{17}$$

The normal modes have the form of plane waves that vary in space and time as $\exp[\mathrm{i}(\boldsymbol{q} \cdot \boldsymbol{r} - \omega t)]$, where $\boldsymbol{q}$ is the wave vector and ω the angular frequency. In an isotropic medium, the normal modes may be separated into transverse and longitudinal ones. In the long-wavelength limit $q \to 0$, the normal modes all have a soundlike dispersion relation, with $\omega = vq$, v being the mode speed. The speed of the two transverse lattice modes is given by [10,11]

$$v_t = \sqrt{\frac{S}{\rho_{\mathrm{I}}}}. \tag{18}$$

Due to interactions between neutron and proton densities and currents, the BA bosons of the neutron superfluid with velocity v_ϕ are mixed with the longitudinal lattice phonons with velocity v_ℓ. Neglecting the coupling of the neutron superfluid to the strain field, the resulting dispersion relation is given by [11,12]

$$\left(\omega^2 - v_\phi^2 q^2\right)\left(\omega^2 - v_\ell^2 q^2\right) = g_{\mathrm{mix}}^2 \omega^2 q^2, \tag{19}$$

where the strength of the mixing is characterized by the parameter

$$g_{\mathrm{mix}} = v_\phi \sqrt{\frac{n_n^{\mathrm{b}}}{n_p + n_n^{\mathrm{b}}} \frac{n_n^{\mathrm{b}}}{n_n^{\mathrm{c}}}}, \tag{20}$$

first introduced in Ref. [12]. The velocity of the BA mode is

$$v_\phi = \sqrt{\frac{n_n^{\mathrm{c}}}{m} \frac{\partial \mu_n}{\partial n_n}}, \tag{21}$$

whereas the velocity of the longitudinal mode of the lattice is

$$v_\ell = \sqrt{\frac{\widetilde{K} + 4S/3}{\rho_{\mathrm{I}}}}. \tag{22}$$

In the neutron-star crust, the electron contribution to the bulk modulus dominates, and the ion contribution can be safely neglected (see, e.g., Sec. 7.1 of Ref. [1]). As a result, v_ℓ is approximately given by [19]

$$v_\ell \approx \frac{\omega_p}{q_{\mathrm{TFe}}} = \sqrt{\frac{n_p}{n_p + n_n^{\mathrm{b}}} \frac{n_p}{m} \frac{\partial \mu_e}{\partial n_e}}. \tag{23}$$

Solving Eq. (14) we find that the eigenmode velocities are given by

$$v_\pm = \frac{V}{\sqrt{2}} \sqrt{1 \pm \sqrt{1 - \frac{4 v_\ell^2 v_\phi^2}{V^4}}}, \tag{24}$$

where

$$V = \sqrt{v_\ell^2 + v_\phi^2 + g_{\mathrm{mix}}^2}. \tag{25}$$

The speed of the transverse lattice phonon in Eq. (18) is unaffected by mixing and is approximately given by [20]

$$v_t \approx 0.4 \frac{\omega_p}{q_{\mathrm{D}}} \approx 0.12 \left(\frac{Z}{50}\right)^{1/3} v_\ell. \tag{26}$$

Note that due to entrainment effects, the expressions (21), (23), and (26) for the velocities of the BA bosons and lattice phonons differ from those obtained considering either a neutron superfluid alone or a pure solid crust, respectively. The self-consistent inclusion of entrainment is an important new element of this study.

In the normal phase, any relative motion between the neutron liquid and the crust will be damped by collisions so in the hydrodynamic regime ions, electrons, and neutrons will be essentially comoving. In this case, the Josephson's equation have to be replaced by the condition $\delta \boldsymbol{v_n} = \delta \boldsymbol{v_p}$. As a result, only one longitudinal mode corresponding to ordinary hydrodynamic sound persists and its velocity is given by

$$c_s = \sqrt{\frac{K + 4S/3}{\rho}}, \tag{27}$$

where K is the total bulk modulus of the crust. It is related to the bulk modulus $\tilde{K}$ of the electron-ion system by

$$K = \widetilde{K} + 2 n_n L + n_n^2 \frac{\partial \mu_n}{\partial n_n}. \tag{28}$$

Since $S \ll K$ (see, e.g., Sec. 7.1 of Ref. [1]), the sound velocity can be approximately written as

$$c_s \approx \sqrt{\frac{\partial P}{\partial \rho}} \approx \sqrt{\frac{n_p}{n} \frac{n_p}{m} \frac{\partial \mu_e}{\partial n_e} + \frac{n_n}{n} \frac{n_n}{m} \frac{\partial \mu_n}{\partial n_n}}. \tag{29}$$

The transverse mode velocity is given by

$$v_t = \sqrt{\frac{S}{\rho}}. \tag{30}$$

While the existence of two weakly damped longitudinal modes is unique to the superfluid phase, entrainment is fairly insensitive to superfluidity provided the pairing gap $\Delta \ll \mu_n$ [21], which is the case in most of the inner crust [22–24].

IV. MICROSCOPIC MODEL FOR THE INNER CRUST OF A NEUTRON STAR

The evaluation of the velocities of the collective modes requires the knowledge of the susceptibilities defined by $\partial n_e / \partial \mu_e$ and $\partial n_n / \partial \mu_n$, and number densities n_p and n_n^{b} for each given baryon density n. At densities above $\sim 10^6$ g cm^{-3}, electrons can be treated as an ideal relativistic Fermi gas so

$$\frac{\partial n_e}{\partial \mu_e} \approx \frac{3 n_e}{\mu_e}. \tag{31}$$

Electric charge neutrality requires $n_e = n_p$ so both n_p and $\partial n_e / \partial \mu_e$ are uniquely determined by the composition of the

inner crust (i.e., the variation of the electron density n_e with n), taken from Ref. [3]. The inner crust was assumed to be made of "cold catalyzed matter," i.e., matter in full thermodynamic equilibrium at zero temperature. Nuclei were supposed to be spherical, an assumption that is generally satisfied in all regions of the inner crust, except possibly near the crust-core interface where so-called nuclear "pastas" might exist (see, e.g., Sec. 3.3 in Ref. [1] for a brief review). The composition of the crust was obtained from a nonrelativistic Skyrme effective nuclear Hamiltonian solved using the fourth-order extended Thomas-Fermi method with proton quantum shell effects added via the Strutinsky-Integral theorem. Neutron quantum shell corrections, which were shown to be much smaller than proton quantum shell corrections [25,26], were neglected. This so-called ETFSI method is a high-speed approximation to the self-consistent Skyrme-Hartree-Fock equations [27]. These calculations were carried out with the Skyrme force BSk14 underlying the HFB-14 atomic mass model [28], which yields an excellent fit to essentially all experimental atomic mass data with a root-mean-square deviation of 0.73 MeV. At the same time, an optimal fit to charge radii was ensured. Moreover, the incompressibility K_v of symmetric nuclear matter at saturation was required to fall in the experimental range 240 ± 10 MeV [29]. The symmetry energy J and its slope L play a crucial role for determining the structure of neutron-star crusts [30]. The values predicted by the force BSk14, $J = 30$ MeV, and $L = 44$ MeV, respectively, are consistent with various constraints inferred from both experiments and astrophysical observations [31]. For these reasons, the force BSk14 is expected to be well suited for describing the nuclei in the inner crust of a neutron star. In addition, the BSk14 force was constrained to reproduce various properties of homogeneous nuclear matter as obtained from many-body calculations using realistic two- and three-nucleon interactions. In particular, the force BSk14 was fitted to the equation of state of neutron matter, as calculated by Friedman and Pandharipande [32] using realistic two- and three-body forces. Incidentally, this equation of state is in good agreement with more recent *ab initio* calculations [33–36] at densities relevant to the neutron-star crusts, as shown in Fig. 1. Therefore, the properties of the neutron liquid in the inner crust of a neutron star are well described by the Skyrme force BSk14. The crustal composition obtained in Ref. [3] is summarized in Table I.

As discussed in detail in an accompanying paper [9], neutron band-structure calculations are needed to determine $n_n^{\rm c}$. Here, we note that the key ingredient is the single-particle (s.p.) dispersion relation $\varepsilon_{\alpha \boldsymbol{k}}$ (α being the band index and $\boldsymbol{k}$ the Bloch wave vector) given by the solution of the Schrödinger equation with the periodic mean-field potential obtained self-consistently from the ETFSI method. The superfluid density was then found from the equation

$$n_n^{\rm c} = \frac{m}{24\pi^3\hbar^2} \sum_\alpha \int_{\rm F} |\boldsymbol{\nabla}_{\boldsymbol{k}} \varepsilon_{\alpha \boldsymbol{k}}| d\mathcal{S}^{(\alpha)}, \tag{32}$$

where $d\mathcal{S}^{(\alpha)}$ is an infinitesimal area element of the piecewise Fermi surface associated with the α band. As described in Ref. [9], in most regions of the inner crust only a small fraction of dripped neutrons contributes to the superfluid density due to

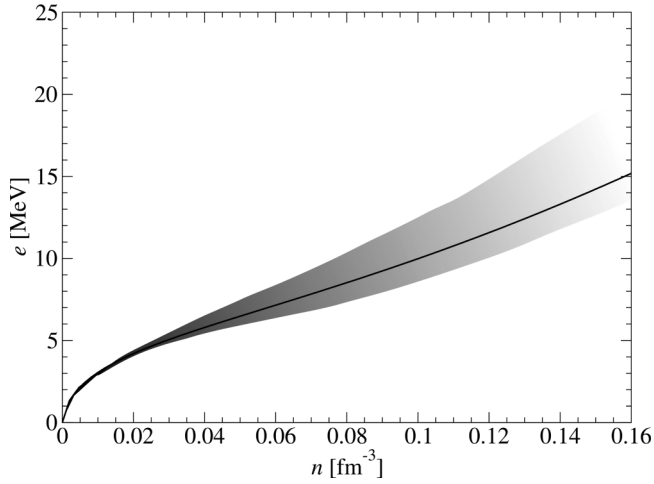

FIG. 1. Energy per baryon in pure neutron matter as calculated by the Skyrme force BSk14 [28] (solid line) and as obtained from next-to-next-to-next-to-leading order in chiral effective field theory [36] (shaded area).

Bragg scattering so $n_n^{\rm c} \ll n_n^{\rm f}$ or, equivalently, $A^\star \approx A_{\rm cell}$. Note that unbound (bound) neutrons with density $n_n^{\rm f}$ (respectively, $n_n - n_n^{\rm f}$) are characterized by s.p. energies $\varepsilon_{\alpha \boldsymbol{k}}$ lying above (respectively, below) the largest value of the periodic mean-field potential. Results are summarized in Table I.

The neutron chemical potential is determined by the neutron band structure from the equation

$$n_n = \int_{-\infty}^{\mu_n} d\varepsilon D(\varepsilon), \tag{33}$$

where $D(\varepsilon)$ is the density of neutron s.p. states defined by

$$D(\varepsilon) = \sum_\alpha \int \frac{d^3\boldsymbol{k}}{(2\pi)^3} \delta(\varepsilon - \varepsilon_{\alpha \boldsymbol{k}}), \tag{34}$$

where the $\boldsymbol{k}$-space integration is taken over the first Brillouin zone. Differentiating Eq. (33) with respect to μ_n thus yields

TABLE I. Ground-state composition of the inner crust of a neutron star (Z, $A_{\rm cell}$, and A as defined in Sec. II), as obtained in Ref. [3], for various baryon densities n/mass densities ρ. The effective number of bound nucleons $A^\star$ was calculated including band-structure effects in Ref. [9]. The density $n_n^{\rm b}$ of effectively bound neutrons can be obtained from Eq. (2). The density of conduction neutrons can be found from Eq. (1).

n (fm^{-3})	ρ (g cm^{-3})	Z	$A_{\rm cell}$	A	$A^\star$
0.0003	4.98×10^{11}	50	200	170	175
0.001	1.66×10^{12}	50	460	179	383
0.005	8.33×10^{12}	50	1140	198	975
0.01	1.66×10^{13}	40	1215	170	1053
0.02	3.32×10^{13}	40	1485	180	1389
0.03	4.98×10^{13}	40	1590	173	1486
0.04	6.66×10^{13}	40	1610	216	1462
0.05	8.33×10^{13}	20	800	87	586
0.06	1.00×10^{14}	20	780	85	461
0.07	1.17×10^{14}	20	714	76	302
0.08	1.33×10^{14}	20	665	65	247

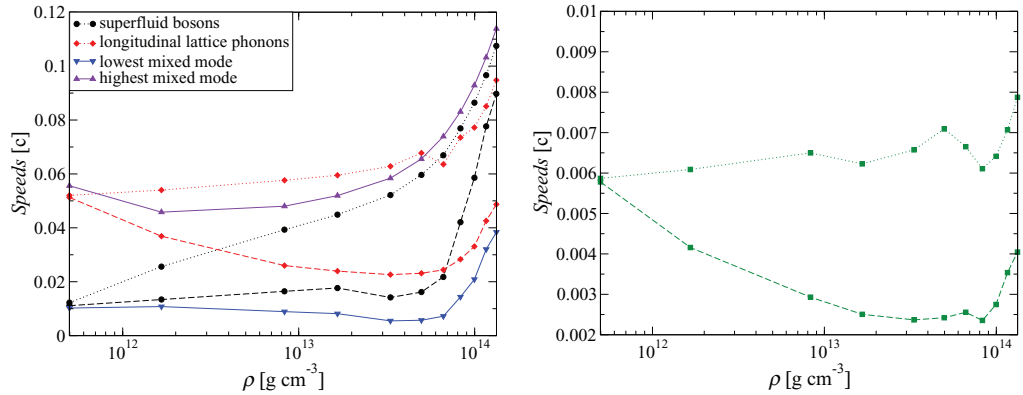

FIG. 2. (Color online) Speeds (in units of the speed of light c) of the longitudinal (left panel) and transverse (right panel) collective excitations in the inner crust of a neutron star. Dotted curves show results with neither mixing nor entrainment, dashed curves include effects due to entrainment only, and solid curves include in addition the effects due to mixing.

the neutron number susceptibility

$$\frac{\partial n_n}{\partial \mu_n} = D(\mu_n) + \int_{-\infty}^{\mu_n} d\varepsilon \frac{\partial D(\varepsilon)}{\partial \mu_n}. \tag{35}$$

Because nuclei in the inner crust are neutron saturated, the neutron susceptibility is essentially independent of the neutron bound states except possibly in a small region close to neutron drip. For the reasons explained in Ref. [37], the density $D(\varepsilon)$ of neutron unbound states in a given region of the inner crust is well approximated by the density of s.p. states in uniform neutron matter for the corresponding density $n_n^{\rm f}$ of dripped neutrons. Using these approximations, the velocity of the BA mode in the inner crust can be expressed as

$$v_\phi = \sqrt{\frac{n_n^{\rm c}}{n_n^{\rm f}}} v_\phi^{\rm f}, \tag{36}$$

where $v_\phi^{\rm f}$ is the velocity of the BA mode in pure neutron matter at the density $n_n^{\rm f}$ associated with the crustal layer under consideration. This latter velocity is given by [38]

$$v_\phi^{\rm f} = \frac{v_{\rm F}^2}{3}(1+F_0)\left(1+\frac{F_1}{3}\right), \tag{37}$$

where $v_{\rm F}$ is the Fermi velocity in pure neutron matter at the density $n_n^{\rm f}$ while F_0 and F_1 are the corresponding dimensionless Landau parameters, whose expressions for Skyrme interactions can be found in Ref. [39]. We have evaluated $v_\phi^{\rm f}$ using the same Skyrme effective interaction BSk14 as that used to determine the equilibrium composition of the crust.

The speeds of the collective modes in the inner crust of a neutron star are shown in Fig. 2 and listed in the Table II. Entrainment modifies the spectrum, v_ϕ, v_ℓ, and v_t are all significantly reduced (compare dotted and dashed curves), and mixing leads to a strong splitting between the longitudinal eigenmodes (note the difference between speeds of the lowest and highest eigenmodes). With increasing density, a strong suppression of the plasma frequency due to entrainment leads to rapid decrease in the velocity of transverse and longitudinal lattice phonon modes. Mixing between longitudinal modes leads to a high velocity eigenmode with velocity v_+ and a low velocity mode with velocity v_-. The v_- mode is predominantly the superfluid phonon (BA) mode near neutron drip and transforms to a mode with a large lattice component at the crust-core boundary. The mode with velocity v_+ is a pure lattice mode at neutron drip and transforms to being a mode which is predominantly a superfluid mode at the crust-core interface.

TABLE II. Properties of collective modes in the inner crust of a neutron star. The velocities (v_ϕ, v_ℓ, c_s, v_t, v_-, and v_+) and the mixing parameter $g_{\rm mix}$ are defined in Sec. III; c is the speed of light. Values in parenthesis are obtained by neglecting entrainment. The ratios of the mean free path of the longitudinal modes to that of the unmixed longitudinal lattice phonon are shown in the last two columns.

n (fm^{-3})	$g_{\rm mix}$ ($10^{-2}c$)	v_ϕ ($10^{-2}c$)	v_ℓ ($10^{-2}c$)	c_s ($10^{-2}c$)	v_t ($10^{-2}c$)	v_- ($10^{-2}c$)	v_+ ($10^{-2}c$)	λ_-/λ_ℓ	λ_+/λ_ℓ
0.0003	2.11	1.11(1.22)	5.13(5.21)	5.35	0.58(0.59)	1.02	5.56	32.3	1.09
0.001	2.60	1.34(2.56)	3.69(5.40)	4.46	0.42(0.61)	1.08	4.58	9.12	1.28
0.005	3.79	1.64(3.93)	2.60(5.76)	4.78	0.29(0.65)	0.89	4.80	3.98	2.02
0.01	4.34	1.77(4.49)	2.39(5.95)	5.18	0.25(0.62)	0.81	5.20	3.63	2.40
0.02	5.22	1.42(5.21)	2.26(6.28)	5.84	0.24(0.66)	0.55	5.84	4.80	2.74
0.03	5.95	1.62(5.97)	2.31(6.78)	6.55	0.24(0.71)	0.57	6.56	4.59	3.01
0.04	6.67	2.18(6.69)	2.44(6.36)	7.39	0.26(0.67)	0.72	7.39	3.76	3.29
0.05	6.73	4.21(7.69)	2.83(7.35)	8.30	0.24(0.61)	1.44	8.31	2.16	3.84
0.06	6.73	5.86(8.65)	3.31(7.72)	9.28	0.28(0.64)	2.09	9.29	1.72	4.45
0.07	6.20	7.76(9.66)	4.26(8.51)	10.3	0.35(0.71)	3.21	10.3	1.45	5.06
0.08	6.34	8.98 (10.9)	4.87(9.48)	11.4	0.40(0.79)	3.84	11.4	1.37	5.50

With increasing temperatures, the neutron superfluidity may disappear in some regions of the crust. In these regions, the two longitudinal modes will merge and give rise to ordinary sound as discussed at the end of Sec. III. Note, however, that the values for the speeds of collective excitations indicated in Table II are expected to remain essentially the same for temperatures $T \lesssim 10^{10}$ K. Indeed, as shown in Ref. [3], thermal effects have a minor impact on the equilibrium composition of neutron-star crusts in this temperature range. However, the crust of a real neutron star may not necessarily be in full thermodynamic equilibrium, as discussed, e.g., in Sec. 3.4 of Ref. [1]. This could affect the spectrum of collective modes.

V. DISSIPATION

Lattice phonons couple strongly to electrons and easily excite electron-hole pairs in the dense electron gas. This Landau damping of lattice phonons has been studied in Ref. [40] and an approximate result of the lattice phonon mean free path was obtained. The mean free path of a thermal phonon that contributes to thermal conductivity was found to be

$$\lambda_{\rm lph} = \frac{6\pi}{Ze^2\gamma\bar{v}}\frac{1}{q_{\rm D}}\frac{F(T_p/T)}{\Lambda_{\rm ph-e}} \simeq 72.5\left(\frac{40}{Z}\right)^{2/3}\left[\frac{F(T_p/T)}{\bar{v}\Lambda_{\rm ph-e}}\right] r_{\rm cell}, \quad (38)$$

where

$$F(T_p/T) = 0.014 + \frac{0.03}{\exp\left[T_p/(5T)\right]+1}, \quad (39)$$

$$\Lambda_{\rm ph-e} = \ln\left(\frac{2}{\gamma}\right) - \frac{1}{2}\left(1-\frac{\gamma^2}{4}\right) \quad \text{and} \quad \gamma = q_{\rm D}/k_{\rm Fe}, \quad (40)$$

and $\bar{v}$ is average velocity of the lattice phonon. Note that for simplicity we have neglected corrections due to the Debye-Waller factor and the nuclear form factor to the Coulomb logarithm $\Lambda_{\rm ph-e}$. Such corrections tend to increase the mean free path and Eq. (38) therefore must be viewed as a lower limit.

Our interest here is to investigate the mean free path of the superfluid phonon mode in the inner crust. In Ref. [41] it was shown that phonon-phonon and phonon-impurity scattering were negligible compared to the dissipation that arose due to mixing with the lattice phonon. The superfluid phonon mean free path, without the inclusion of entrainment effects, was found to be much larger than that of the lattice phonons because mixing due to the density interaction was weak. In the following, we include effects due to entrainment, which is now known to be the dominant contribution to the mixing parameter $g_{\rm mix}$, and we show that the mean free path of the superfluid mode is greatly reduced due to strong mixing. Incorporating this into the dispersion relation in Eq. (19) we obtain

$$\left(\omega^2 - v_\phi^2 q^2\right)\left(\omega^2 - 2{\rm i}\Gamma_\ell\omega - v_\ell^2 q^2\right) = g_{\rm mix}^2\omega^2 q^2, \quad (41)$$

where $\Gamma_\ell = v_\ell/\lambda_\ell$ and λ_ℓ is the mean free path of the lattice phonon in the limit of weak damping ($\Gamma_\ell \ll v_\ell q$). In general, $\lambda_\ell \neq \lambda_{\rm lph}$ as the latter is an average mean free path more closely related to the mean free path of the transverse thermal phonon. Nonetheless it provides an order of magnitude estimate.

Mode mixing induces an indirect coupling between the superfluid BA bosons and electrons. Because the longitudinal modes contain an admixture of superfluid and lattice phonons, the damping of lattice vibrations due to electron-hole excitations naturally leads to a finite damping of both modes. In a small region of the crust in the vicinity of the neutron-drip transition where $g_{\rm mix}^2 \ll v_\ell^2 - v_\phi^2$ the modes are not strongly mixed, and, using the fact that $v_\ell \gg v_\phi$, we can obtain from Eq. (41) the analytic relation

$$\lambda_\phi \approx \frac{v_\ell^3}{g_{\rm mix}^2 v_\phi}\lambda_\ell = \left(\frac{v_\ell}{v_\phi}\right)^3 \frac{n_n^{\rm c}\left(n_p + n_n^{\rm b}\right)}{\left(n_n^{\rm b}\right)^2}\lambda_\ell \gg \lambda_\ell \quad (42)$$

between the mean free paths of the superfluid and lattice modes. In other regions mixing is strong and damping associated with each eigenmodes is found by solving Eq. (41). Although an analytic solution exists, it is cumbersome to write down explicitly. We present numerical values for the ratio of the mean free paths λ_+/λ_ℓ and λ_-/λ_ℓ where $\lambda_\pm$ are the mean free paths of the eigenmodes in the last two columns of Table II. It is meaningful to calculate these ratios without specifying λ_ℓ because it is independent of λ_ℓ in the weak damping limit. From the table we see that the mean free path of the mode with a large superfluid component is large near neutron drip but decreases rapidly due to mixing when $v_\ell \simeq v_\phi$. In the bulk of the inner crust both modes have comparable mean free paths and this behavior qualitatively differs from that observed in Ref. [41] where entrainment was neglected and mixing was found to be weak except in a narrow region close to resonance.

VI. IMPLICATIONS

X-ray observations of accreting neutron stars in low-mass x-ray binaries have recently proved to be very useful for probing neutron-star interiors. The accretion of matter onto the surface of the neutron star triggers thermonuclear fusion reactions. Under certain circumstances, these reactions can become explosive, giving rise to x-ray bursts and superbursts [42]. The ignition conditions of these thermonuclear flashes depend sensitively on the thermal properties of the crust. Valuable information on neutron star crusts can also be obtained from the thermal x-ray emission in quiescence following a long outburst of accretion during which the crust has been driven out of its thermal equilibrium with the core [43]. The thermal relaxation between the accreting and quiescent stages has been monitored for the four quasipersistent soft x-ray transients KS 1731−260 [44], MXB 1659−29 [45], XTE J1701−462 [46], and EXO 0748−676 [47]. Numerical simulations of these phenomena have shown that the cooling is very sensitive to the properties of the neutron-star crust [43,48,49]. In particular, the thermal relaxation time of the crust is approximately given by [50,51]

$$\tau \sim (\Delta R)^2\left(1-\frac{2GM}{Rc^2}\right)^{-3/2}\frac{C_V}{\kappa}, \quad (43)$$

where ΔR is the crust thickness, R is the radius, and M is gravitational mass of the neutron star, while C_V and κ are the

average heat capacity and thermal conductivity in the density range between $\sim 0.1\,\bar{n}_{\rm cc}$ and $\bar{n}_{\rm cc}$, where $\bar{n}_{\rm cc} = 0.08$ fm^{-3} is the crust-core transition density. The thermal relaxation of hot newly born neutron stars could also shed light on the crust properties. However, such very young neutron stars have not been observed yet, being presumably obscured by their expanding supernova envelope.

The inner crust heat capacity is the sum of contributions from the quasiparticle excitations of the electron gas and neutron liquid and from the collective excitations described above. In what follows, we describe these contributions to the volumetric crustal heat capacity. Treating electrons as a relativistic Fermi gas, their heat capacity is simply given by ($k_{\rm B}T \ll \mu_e$)

$$C_V^e = \frac{1}{3}\frac{\mu_e^2}{(\hbar c)^3} k_{\rm B} T. \tag{44}$$

The heat capacity of nonsuperfluid degenerate neutrons (for $k_{\rm B}T \ll \mu_n$) is similarly given by

$$C_V^n = \tfrac{1}{3}\pi^2 D(\mu_n) k_{\rm B} T, \tag{45}$$

where $D(\mu_n)$ is well approximated by the density of states in uniform neutron matter at the density $n_n^{\rm f}$ [37]. This neutron contribution is enormous and will always dominate in the layers where neutrons are normal. Once superfluidity sets in, however, C_V^n is strongly suppresssed and becomes negligible when the temperature is much lower than the critical temperature T_c^n [23,24]. Given the density dependence of the neutron $^1S_0$ gap there are only two regions, just above the neutron drip point and possibly in the deepest part of the crust, where C_V^n is relevant (see, e.g., Ref. [13]).

The heat capacity associated with a collective excitation having a dispersion relation of the form $\omega = vq$ is given by

$$C_V^{\rm coll} = \frac{3n_p}{Z x_D^3}\int_0^{x_D} dx \frac{x^4 e^x}{(e^x-1)^2}, \tag{46}$$

with $x_D = \Theta_D/T$, $\Theta_D = (\hbar/k_{\rm B})\, q_D v$ being the Debye temperature of the collective mode. At low temperatures, $T \ll \Theta_D$ such that $x_D \gg 1$, one has the standard Debye result

$$C_V^{\rm coll} \simeq \frac{2\pi^2}{15}\left(\frac{k_{\rm B}T}{\hbar v}\right)^3 = n_{\rm I}\frac{4\pi^4}{5}\left(\frac{k_{\rm B}T}{\hbar q_D v}\right)^3 \tag{47}$$

while at high temperatures, $T \gg \Theta_D$ when $x_D \ll 1$, one obtains the classical result $C_V^{\rm coll} = n_{\rm I}$. At low-enough temperatures ($T \ll \Theta_D$ and $T \ll T_c^n$) the heat capacity of the crust is, hence, approximately given by

$$C_V \simeq \frac{1}{3}\frac{\mu_e^2}{(\hbar c)^3} k_{\rm B} T + \frac{2\pi^2}{15}\left(\frac{k_{\rm B}T}{\hbar \bar{v}}\right)^3, \tag{48}$$

with

$$\frac{1}{\bar{v}^3} = \frac{2}{v_t^3} + \frac{1}{v_-^3} + \frac{1}{v_+^3}. \tag{49}$$

We plot in Fig. 3 the Debye temperatures of the four collective modes and the various contributions to C_V are displayed in Figs. 4–6 for three typical temperatures of astrophysical interest. While at $T = 10^9$ K, the v_- mixed mode and the two degenerate transverse modes are in the classical regime, all modes are well into the quantum regime at $T = 10^8$ K and $T = 10^7$ K. This suggests that entrainment and mixing will not affect the thermal relaxation of newly born isolated neutron stars but could be important for accreting neutron stars.

Figures 4–6 show that the heat capacity of nonsuperfluid neutrons would largely dominate over all collective modes but becomes insignificant once neutron superfluidity sets in, i.e., in most of the inner crust. Overall, the transverse lattice mode contribution C_V^t to the heat capacity dominates at $T = 10^9$ K and 10^8 K, while electrons dominate at 10^7 K due to the linear temperature dependence of C_V^e compared to the T^3 dependence for C_V^t. C_V^t in not affected by entrainment at $T = 10^9$ K, since the transverse modes are in the classical regime, but at $T = 10^8$ K and 10^7 K it is increased by almost one order of magnitude in most of the crust. Notice that at $T = 10^8$ K without entrainment C_V^t would be comparable to

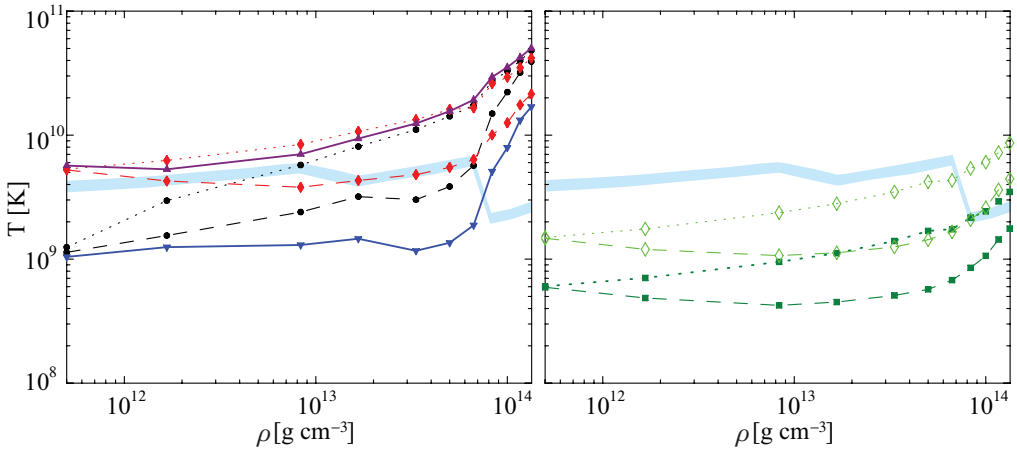

FIG. 3. (Color online) Left panel: Debye temperatures Θ_D of the longitudinal collective excitations in the inner crust of a neutron star using the same notations as in Fig. 2. Dotted curves show values with neither mixing nor entrainment, dashed curves include effects due to entrainment only and solid curves include in addition the effects due to mixing. Right panel: Debye temperature Θ_D of the transverse collective modes (lines with filled squares) and ion plasma temperature $T_p = (\hbar/k_{\rm B})\omega_p$ (lines with diamonds). Dotted (dashed) curves show values without (with) entrainment. In both panels, the light blue band delimits the range of T below which nuclei crystalize (using $\Gamma_c = 180$ to 220).

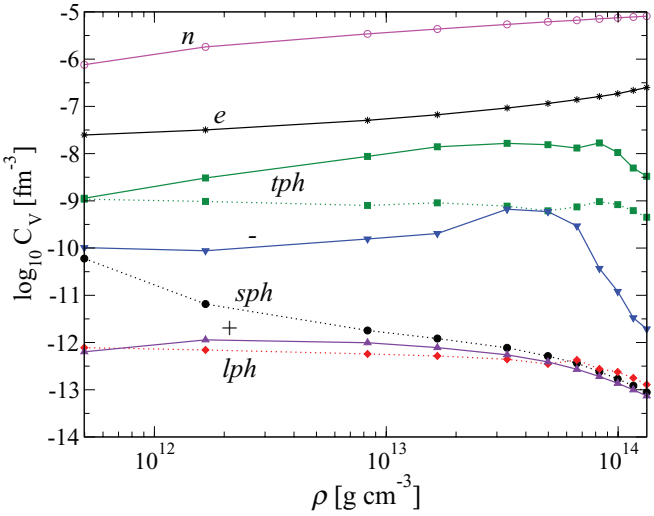

FIG. 4. (Color online) Heat capacity of electrons (e), transverse lattice phonons (tph) and longitudinal excitations ($-$ and $+$) in the inner crust of neutron stars at $T = 10^7$ K, with mixing and entrainment effects (solid lines) and without (dotted lines). In the absence of mixing, the longitudinal modes are the Bogoliubov-Anderson superfluid phonons (sph) and the longitudinal lattice phonons (lph). For comparison, is also shown the normal neutron contribution (n), but it is strongly suppressed by superfluidity except in the shallowest and densest parts of the inner crust where the neutron $^1S_0$ pairing gap becomes vanishingly small.

C_V^e while it clearly dominates once entrainment is taken into account. Moreover, the heat capacity of the longitudinal mode is increased by several orders of magnitude by entrainment and mixing. In particular, the contribution of the lowest mixed mode becomes even comparable with C_V^e at high temperatures.

Because entrainment modifies the spectrum of collective excitations, it also affects the heat transport in the crust. The thermal conductivity is generally governed by electrons. Changes of phonon velocities alter the electron-phonon process hence also the electron thermal conductivity. The

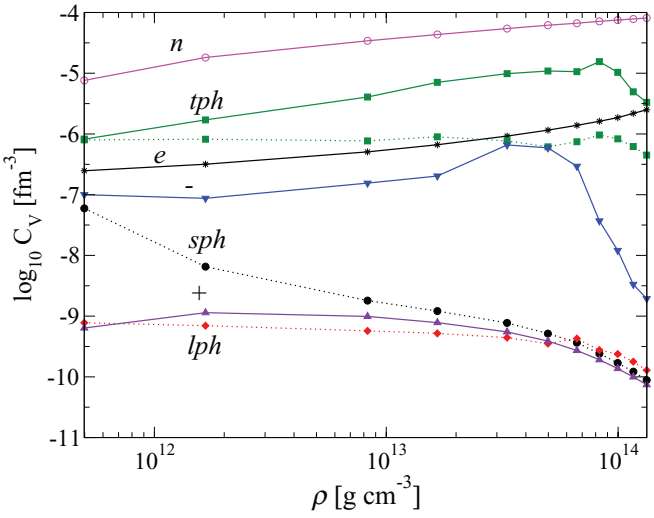

FIG. 5. (Color online) Same as Fig. 4 for $T = 10^8$ K.

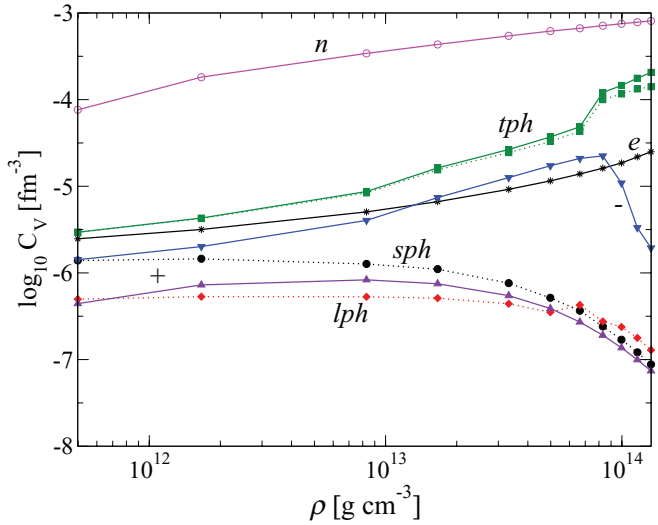

FIG. 6. (Color online) Same as Fig. 4 for $T = 10^9$ K.

conductivity is mainly limited by the Umklapp process, in which an electron simultaneously Bragg scatters off the lattice and emits a transverse phonon [52,53]. Since the scattering rate scales as v^{-3}, where v is the phonon velocity, and $v_\ell \gg v_t$, processes involving longitudinal phonons are typically negligible. This observation also permits us to reliably estimate the changes in the electron mean free path due to entrainment. First, we note that the electron-phonon scattering rate depends on the electron Fermi momentum $k_{\rm Fe}$, the ion plasma frequency ω_p, and v_t (see Ref. [13] for a discussion). Since $v_t \propto \omega_p/q_{\rm D}$, it follows that effects due to entrainment on the scattering are entirely incorporated through its effects on ω_p. It therefore suffices to employ an existing fitting formula developed in an earlier work but with a suitably reduced value of ω_p due to entrainment. In Fig. 7 we plot the electron thermal conductivity with and without entrainment effects included. As anticipated, the conductivity decreases with entrainment simply reflecting

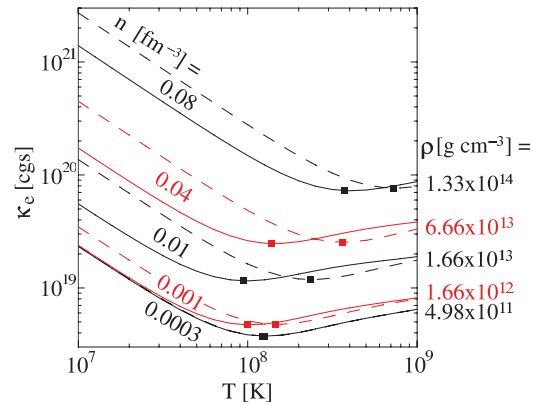

FIG. 7. (Color online) Electron thermal conductivity κ_e in the inner crust of a neutron star, with (solid) and without (dashed) entrainment effects included, at five densities, $n = 0.0003$, 0.001, 0.01, 0.02, and 0.08 fm^{-3} as labeled on the curves. The minimum of κ_e occurs at $T \sim 0.1T_p$, marked by a square on the corresponding curve, $\kappa_e \propto T^{-1}$ in the quantum regime, $T \ll T_p$, while it only weakly increases with T in the classical regime at higher temperatures.

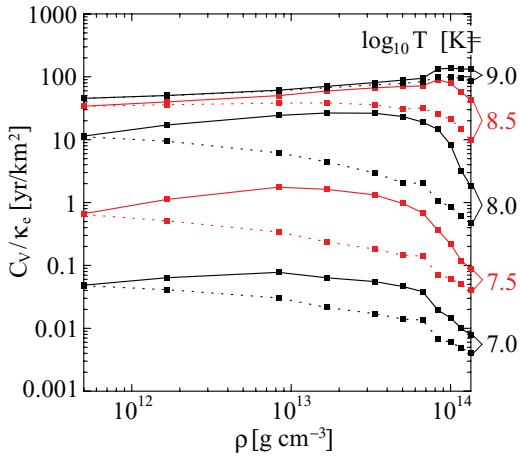

FIG. 8. (Color online) Ratio of the heat capacity C_V to the electron thermal conductivity κ_e at five temperatures, as labeled. C_V includes the ion as well as the electron contributions, the neutron part is neglected. Continuous lines show values when entrainment, through its modification of T_p, is taken into account, while in the values for dotted lines it is neglected.

the fact that it is easier to excite lower velocity transverse phonon modes.

Having described the impact of entrainment on reducing the electron thermal conductivity and increasing the lattice specific heat, we now discuss their combined effect on the thermal time scale, Eq. (42). We plot C_V/κ in Fig. 8 for five different temperatures. For $T = 10^9$ K, the impact of entrainment is negligible since T is comparable or larger than Θ_D of the transverse modes, as already pointed out previously. As the temperature is decreased, entrainment leads to a significant enhancement in C_V/κ, hence also in τ : at $\rho = 10^{13}$ g cm^{-3} and for $T = 10^8$ K, τ can be increased by more than one order of magnitude. For $T = 10^7$ K, the lowest temperature considered here, the effect of entrainment is smaller, being moderated by the dominance of the electron contribution to C_V.

Although electrons dominate heat conduction under normal conditions, phonons can contribute either at high temperature when $C_V^{\rm coll} \geqslant C_V^e$ or when large magnetic fields suppress electron conduction transverse to the field [40,41]. In the inner crust, the lattice and superfluid phonons contributions were estimated in Refs. [40] and [41], respectively. From kinetic theory and in the case where phonon conduction is diffusive (rather than convective), the thermal conductivity is given by

$$\kappa^{\rm coll} = \tfrac{1}{3} C_V^{\rm coll} v \lambda, \tag{50}$$

where $C_V^{\rm coll}$ is the heat capacity, v is the velocity, and λ is the mean free path of each collective mode. Entrainment alters the thermal conductivity through these three factors. The larger specific heat associated with lower velocity transverse modes implies that their contribution to the heat conduction is proportionately enhanced. In addition, since $\lambda \propto 1/v$, the smaller v_t acts to further increase the conductivity, and the combined effect is to increase the earlier estimate of Ref. [40] by the factor $(A^\star/A)^{3/2}$.

The effects on the superfluid phonon contribution is more complex because mixing is strong throughout the inner crust except in the vicinity of neutron drip. It is only meaningful to discuss heat diffusion due to eigenmodes, and, in general, there are two competing effects due entrainment. At first entrainment lowers the velocity of the mode with a larger superfluid component and increases its heat capacity, but with increasing density this increase is overcome by strong mixing which dramatically reduces the mean free path. Since λ_+ and λ_- are of the same magnitude as λ_ℓ, and because $v_+ \gg v_t$ and $v_- \gg v_t$, their contribution to heat transport is typically negligible. This new result implies that superfluid modes may play a smaller role in heat transport in magnetars than anticipated in Ref. [41], and it is likely that the enhanced heat conduction due to the transverse mode will dominate in much of the inner crust.

VII. CONCLUSIONS

A large fraction of dripped neutrons in the inner crust of a neutron star are entrained by nuclei and move with them, due to coherent (Bragg) scattering of neutrons by the crystal lattice [8,9]. This nondissipative entrainment induces a strong coupling between the superfluid and lattice dynamics and is shown to affect the spectrum of low-energy collective excitations of the inner crust. Superfluid and longitudinal lattice phonons are found to be very strongly mixed, and the speed of transverse lattice modes is greatly reduced, thus leading to a significant enhancement of the crustal specific heat at temperatures above $\sim 10^8$ K. This, combined with entrainment induced reduction in the electron mean free path, entails an increase of the heat diffusion time in the crust, especially for temperatures in the range 10^7–10^8 K encountered in quasipersistent soft x-ray transients. This warrants the need to take into account entrainment effects in the interpretation of the observed thermal relaxation in these accreting neutron stars.

Shear modes in neutron-star crusts with velocity in the range $v_t \simeq 10^{-3}$–10^{-2} c have been proposed to play a role in the interpretation of quasiperiodic oscillations (QPOs) observed in giant flares from SGRs [54]. The fundamental frequency of the global shear mode is given by $\Omega_0 \simeq \bar{v}_t/2\pi R$, R being the neutron-star radius and $\bar{v}_t$ an appropriate average of the shear velocity in the inner crust, where the mode energy mainly resides [55]. Since entrainment lowers v_t by a factor of about 2–3 in most of the inner crust, our results suggest that Ω_0 is too small to account for the observed QPO frequencies in the giant flares [56]. It is also likely that the existence of the low-velocity longitudinal eigenmode in the coupled superfluid-solid inner crust may be relevant to interpret global oscillation modes.

However, there are several issues that deserve further attention before one can draw quantitative conclusions from our study. The possible presence of nuclear "pastas" in the deep regions of the inner crust, which has been neglected here, would reduce the effects of Bragg scattering [6] and change the temperature dependence of the specific heat at low temperatures [57] due to the low dimensionality of these configurations. Besides, the composition and the properties of neutron-star crusts may differ from those of cold-catalyzed matter that we have considered in this work. We anticipate that quantum and thermal fluctuations of nuclei about their

equilibrium positions, crystal defects, impurities, and, more generally, any source of disorder would presumably reduce the number of entrained neutrons. Quantitative estimates of all these effects is beyond the scope of this work.

ACKNOWLEDGMENTS

This work was financially supported by FNRS (Belgium) and CompStar, a Research Networking Programme of the European Science Foundation. N.C. thanks the Institute for Nuclear Theory at the University of Washington for its hospitality and the Department of Energy for partial support. The work of S.R. was supported by DOE Grant No. DE-FG02-00ER41132 and by the Topical Collaboration to study neutrinos and nucleosynthesis in hot dense matter. D.P.'s work was supported by grants from Conacyt (Grant No. CB-2009/132400) and UNAM-DGAPA (Grant No. PAPIIT IN113211).

[1] N. Chamel and P. Haensel, Living Rev. Relativity **11**, 10 (2008), http://relativity.livingreviews.org/Articles/lrr-2008-10/.
[2] J. M. Pearson, S. Goriely, and N. Chamel, Phys. Rev. C **83**, 065810 (2011).
[3] M. Onsi, A. K. Dutta, H. Chatri, S. Goriely, N. Chamel, and J. M. Pearson, Phys. Rev. C **77**, 065805 (2008).
[4] J. M. Pearson, N. Chamel, S. Goriely, and C. Ducoin, Phys. Rev. C **85**, 065803 (2012).
[5] M. Baldo, E. E. Saperstein, and S. V. Tolokonnikov, Nucl. Phys. A **749**, 42c (2005).
[6] B. Carter, N. Chamel, and P. Haensel, Nucl. Phys. A **748**, 675 (2005).
[7] B. Carter, N. Chamel, and P. Haensel, Int. J. Mod. Phys. D **15**, 777 (2006).
[8] N. Chamel, Nucl. Phys. A **747**, 109 (2005).
[9] N. Chamel, Phys. Rev. C **85**, 035801 (2012).
[10] N. Andersson, K. Glampedakis, and L. Samuelsson, Mon. Not. R. Astron. Soc. **396**, 894 (2009).
[11] C. J. Pethick, N. Chamel, and S. Reddy, Prog. Theor. Phys. Suppl. **186**, 9 (2010).
[12] V. Cirigliano, S. Reddy, and R. Sharma, Phys. Rev. C **84**, 045809 (2011).
[13] D. Page and S. Reddy, in *Neutron Star Crust*, edited by C. Bertulani and J. Piekarewicz (Nova Science Publishers, 2012), pp. 281–308.
[14] R. I. Epstein, Astrophys. J. **333**, 880 (1988).
[15] N. N. Bogoliubov, V. V. Tolmachev, and D. N. Shirkov, *New Method in the Theory of Superconductivity* (Academy of Sciences of the USSR, Moscow, 1958).
[16] P. W. Anderson, Phys. Rev. **112**, 1900 (1958).
[17] T. Maruyama, T. Tatsumi, D. N. Voskresensky, T. Tanigawa, and S. Chiba, Phys. Rev. C **72**, 015802 (2005).
[18] B. Carter and E. Chachoua, Int. J. Mod. Phys. D **15**, 1329 (2006).
[19] N. W. Ashcroft and N. D. Mermin, *Solid State Physics* (Holt, Rinehart & Winston, 1976).
[20] G. Chabrier. N. W. Ashcroft, and H. E. Dewitt, Nature **360**, 6399 (1992).
[21] B. Carter, N. Chamel, and P. Haensel, Nucl. Phys. A **759**, 441 (2005).
[22] M. Baldo, E. E. Saperstein, and S. V. Tolokonnikov, Eur. Phys. J. A **32**, 97 (2007).
[23] N. Chamel, S. Goriely, J. M. Pearson, and M. Onsi, Phys. Rev. C **81**, 045804 (2010).
[24] M. Fortin, F. Grill, J. Margueron, D. Page, and N. Sandulescu, Phys. Rev. C **82**, 065804 (2010).
[25] K. Oyamatsu and M. Yamada, Nucl. Phys. A **578**, 181 (1994).
[26] N. Chamel, S. Naimi, E. Khan, and J. Margueron, Phys. Rev. C **75**, 055806 (2007).
[27] J. R. Stone and P. G. Reinhard, Prog. Part. Nucl. Phys. **58**, 587 (2007).
[28] S. Goriely, M. Samyn, and J. M. Pearson, Phys. Rev C **75**, 064312 (2007).
[29] G. Colò, N. V. Giai, J. Meyer, K. Bennaceur, and P. Bonche, Phys. Rev. C **70**, 024307 (2004).
[30] F. Grill, C. Providência, and S. S. Avancini, Phys. Rev. C **85**, 055808 (2012).
[31] J. M. Lattimer, Annu. Rev. Nucl. Part. Sci. **62**, 485 (2012).
[32] B. Friedman and V. R. Pandharipande, Nucl. Phys. A **361**, 502 (1981).
[33] A. Akmal, V. R. Pandharipande, and D. G. Ravenhall, Phys. Rev. C **58**, 1804 (1998).
[34] A. Gezerlis and J. Carlson, Phys. Rev. C **81**, 025803 (2010).
[35] K. Hebeler and A. Schwenk, Phys. Rev. C **82**, 014314 (2010).
[36] I. Tews, T. Kruger, K. Hebeler, and A. Schwenk, Phys. Rev. Lett. **110**, 032504 (2013).
[37] N. Chamel, J. Margueron, and E. Khan, Phys. Rev. C **79**, 012801(R) (2009).
[38] A. J. Leggett, Phys. Rev. **147**, 119 (1966).
[39] S. Goriely, N. Chamel, and J. M. Pearson, Phys. Rev. C **82**, 035804 (2010).
[40] A. I. Chugunov and P. Haensel, Mon. Not. R. Astron. Soc. **381**, 1143 (2007).
[41] D. N. Aguilera, V. Cirigliano, J. A. Pons, S. Reddy, and R. Sharma, Phys. Rev. Lett. **102**, 091101 (2009).
[42] T. Strohmayer and L. Bildsten in *Compact Stellar X-Ray Sources*, edited by W. Lewin and M. van der Klis, Cambridge Astrophysics Series 39 (Cambridge University Press, Cambridge, UK, 2006), p. 113.
[43] R. E. Rutledge, L. Bildsten, E. F. Brown, G. G. Pavlov, V. E. Zavlin, and G. Ushomirsky, Astrophys. J. **580**, 413 (2002).
[44] E. M. Cackett, E. F. Brown, A. Cumming, N. Degenaar, J. M. Miller, and R. Wijnands, Astrophys. J. **722**, L137 (2010).
[45] E. M. Cackett, R. Wijnands, J. M. Miller, E. F. Brown, and N. Degenaar, Astrophys. J. **687**, L87 (2008).
[46] J. K. Fridriksson, J. Homan, R. Wijnands, E. M. Cackett, D. Altamirano, N. Degenaar, E. F. Brown, M. Méndez, and T. M. Belloni, Astrophys. J. **736**, 162 (2011).
[47] N. Degenaar, M. T. Wolff, P. S. Ray, K. S. Wood, J. Homan, W. H. G. Lewin, P. G. Jonker, E. M. Cackett, J. M. Miller, E. F. Brown, and R. Wijnands, Mon. Not. R. Astron. Soc. **412**, 1409 (2011).

[48] P. S. Shternin, D. G. Yakovlev, P. Haensel, and A. Y. Potekhin, Mon. Not. R. Astron. Soc. Lett. **382**, L43 (2007).
[49] E. F. Brown and A. Cumming, Astrophys. J. **698**, 1020 (2009).
[50] J. M. Lattimer, K. A. van Riper, M. Prakash, and M. Prakash, Astrophys. J. **425**, 802 (1994).
[51] O. Y. Gnedin, D. G. Yakovlev, and A. Y. Potekhin, Mon. Not. R. Astron. Soc. **324**, 725 (2001).
[52] E. Flowers and N. Itoh, Astrophys. J. **206**, 218 (1976).
[53] M. E. Raikh and D. G. Yakovlev, Astrophys. Space Sci. **87**, 193 (1982).
[54] T. E. Strohmayer and A. L. Watts, Astrophys. J. **653**, 593 (2006).
[55] A. L. Piro, Astrophys. J. **634**, L153 (2005).
[56] A. W. Steiner and A. L. Watts, Phys. Rev. Lett. **103**, 181101 (2009).
[57] L. Di Gallo, M. Oertel, and M. Urban, Phys. Rev. C **84**, 045801 (2011).